MODELLING TURBULENT HEAT FLUXES USING THE ELLIPTIC BLENDING APPROACH FOR NATURAL CONVECTION

F. Dehoux
Fluid Mechanics, Power generation and Environment Department
(MFEE Dept.)
EDF R&D
Chatou, France
frederic.dehoux@edf.fr

S. Benhamadouche
Fluid Mechanics, Power generation and Environment Department
(MFEE Dept.)
EDF R&D
Chatou, France
sofiane.benhamadouche@edf.fr

R. Manceau
Department Fluid flow, Heat Transfer and Combustion
Institut PPRIME
CNRS–Univ. Poitiers–ENSMA, France
remi.manceau@univ-poitiers.fr

ABSTRACT

The present contribution focuses on the modelling of the buoyancy production term in the transport equation for the dissipation of turbulent kinetic energy. The natural convection test case of Versteegh & Nieuwstadt (1999) is considered, which consists in a DNS of a differentially-heated, vertical-channel flow. Consistently with the underlying physics, it is found beneficial, contrary to the usual practise, to separately model the buoyancy and dynamic parts of the production of dissipation, in order to account for the increase of dynamic production and the variations of the thermal-to-mechanical time-scale ratio in the near-wall region.

INTRODUCTION

Many industrial applications, in particular in the field of energy production and including heat transfer phenomena, are still treated with eddy-viscosity models and the Simple Gradient Diffusion Hypothesis (SGDH) for the modelling of turbulent heat fluxes, although the applications span the range of forced convection, mixed and natural convection regimes. In the last few years, the Elliptic Blending Reynolds-Stress Model (EB-RSM, Manceau & Hanjalić, 2002) gave very satisfactory results in several configurations, in particular in isothermal and forced convection applications (Thielen *et al.*, 2005), with, in particular, a correct reproduction of the turbulence anisotropy in the near-wall region. More recently, Shin *et al.* (2008), Lecocq *et al.* (2008) and Dehoux *et al.* (2010, 2011) extended the concept of elliptic blending (EB) to estimate the turbulent heat fluxes. It was shown in Dehoux *et al.* (2011) that the length scale which has to be considered in the elliptic equation for the turbulent heat fluxes is almost twice the one used for the Reynolds stresses. Moreover, the elliptic blending combined with a Generalized Gradient Diffusion Hypothesis (GGDH) or an Algebraic Flux Model (AFM) considerably improved the prediction of the streamwise heat flux in mixed convection regime (fully developed vertical channel flows with buoyancy effects, DNS data of Kasagi & Nishimura, 1997). Although, in simplified, 1D situations, this term does not have a direct impact on the mean temperature, which is driven by the wall-normal heat flux, it can play a major role in the buoyancy production terms and the dissipation transport equation, depending on the situation. Therefore, although the use of the elliptic blending concept for predicting the turbulent heat fluxes is promising, the case of natural convection is more problematic, and, to a large extent, remains an open issue. Figure 1 shows the velocity profiles of the EB-RSM with several heat flux models. It can be seen that all the models dramatically over-estimate the mean velocity, which motivates the present work.

FLOW CONFIGURATION

The widely used test case of Versteegh & Nieuwstadt (1999) is considered first, which consists in a Direct Numerical Simulation of a vertical channel differentially heated without an imposed pressure gradient. The Rayleigh and Prandtl numbers are equal to 5.10^6 and 0.71, respectively. It is worth noting that the velocity has not been made non-dimensional herein using the bulk velocity as in Dol *et al.* (1997), in order to avoid an artificial correction of the results. The overestimation of the velocity is due to the poor prediction of both the Reynolds shear stress and the mean temperature (and thus the buoyancy force in the momentum equations). Several papers focus on the improvement of the prediction of the turbulent heat fluxes and the temperature variance in this case (Dol *et al.*, 1997, among others) but, to the authors knowledge, none of them deals with the treatment of the buoyancy

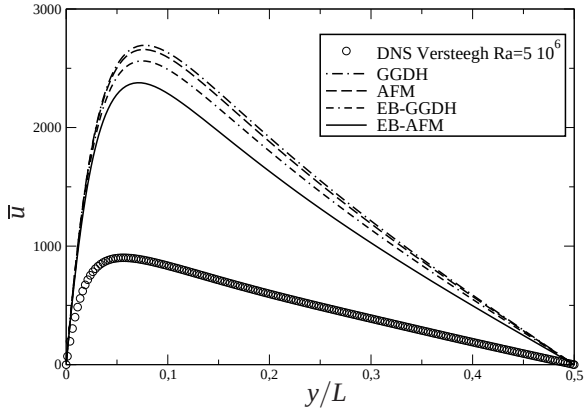

Figure 1. Mean velocity with several heat flux models and a standard time scale in the buoyancy term of ε.

term in the turbulent dissipation equation. The main objective of the present work is thus to improve the modelling of the buoyancy production term in the dissipation equation and, with a particular focus on the time scale.

MODELLING OF THE BUOYANCY PRODUCTION TERM IN THE DISSIPATION EQUATION

Production terms

On the one hand, the exact transport equation for the turbulent dissipation is

$$\begin{aligned}\frac{\mathrm{D}\varepsilon}{\mathrm{D}t} = & \underbrace{-2\nu\left(\overline{\frac{\partial u_i}{\partial x_l}\frac{\partial u_k}{\partial x_l}}+\overline{\frac{\partial u_l}{\partial x_i}\frac{\partial u_l}{\partial x_k}}\right)\frac{\partial U_i}{\partial x_k}}_{P_{\varepsilon1}+P_{\varepsilon2}} \\ & \underbrace{-2\nu u_k\overline{\frac{\partial u_i}{\partial x_l}\frac{\partial^2 U_i}{\partial x_k\partial x_l}}}_{P_{\varepsilon3}}\underbrace{-2\nu\overline{\frac{\partial u_i}{\partial x_l}\frac{\partial u_i}{\partial x_l}\frac{\partial u_k}{\partial x_l}}}_{P_{\varepsilon4}} \\ & \underbrace{-2\nu\beta g_i\overline{\frac{\partial u_i}{\partial x_l}\frac{\partial\theta}{\partial x_l}}}_{G_\varepsilon}\underbrace{-2\overline{\left(\nu\frac{\partial^2 u_i}{\partial x_k\partial x_l}\right)}}_{Y_\varepsilon} \\ & \underbrace{+\frac{\partial}{\partial x_k}\left(\underbrace{-2\frac{\nu}{\rho}\overline{\frac{\partial p}{\partial x_l}\frac{\partial u_k}{\partial x_l}}}_{D^p_\varepsilon}\underbrace{-\overline{\nu u_j\left(\frac{\partial u_i}{\partial x_l}\right)^2}}_{D^t_\varepsilon}+\underbrace{\nu\frac{\partial\varepsilon}{\partial x_k}}_{D^\nu_\varepsilon}\right)}_{D_\varepsilon}\end{aligned} \quad (1)$$

where $P_\varepsilon = P_{\varepsilon1}+P_{\varepsilon2}+P_{\varepsilon3}+P_{\varepsilon4}$ denotes dynamic production, G_ε buoyancy production, D_ε diffusion and Y_ε viscous destruction.

On the other hand, the widely-used model equation for ε is of the form

$$\frac{\mathrm{D}\varepsilon}{\mathrm{D}t} = \underbrace{\frac{\partial}{\partial x_k}\left(\nu\delta_{kl}+\frac{C_S}{\sigma_\varepsilon}TR_{kl}\frac{\partial\varepsilon}{\partial x_l}\right)}_{D_\varepsilon}+\underbrace{C'_{\varepsilon1}\frac{P_k+G_k}{T}}_{P_\varepsilon+G_\varepsilon}-\underbrace{C_{\varepsilon2}\frac{\varepsilon}{T}}_{Y_\varepsilon}, \quad (2)$$

where T is the dynamic time scale, $C_S = 0.21$, $\sigma_\varepsilon = 1.15$, $C_{\varepsilon2} = 1.83$. Since the EB-RSM is a near-wall model, the productions terms $P_{\varepsilon1}$, $P_{\varepsilon2}$ and $P_{\varepsilon3}$ cannot be neglected, such that, the coefficient $C'_{\varepsilon1}$ is made variable (Manceau, 2005)

$$C'_{\varepsilon1} = C_{\varepsilon1}\left[1+A_1^k\left(1-\alpha^3\right)\sqrt{\frac{k}{R_i jn_in_j}}\right], \quad (3)$$

with $A_1^k = 0.023$, $C_{\varepsilon1} = 1.44$, $n_i = \nabla\alpha/\|\nabla\alpha\|$ the unit wall normal vector and α the elliptic blending factor, solution of the elliptic equation

$$\alpha - L^2\nabla^2\alpha = 1, \quad (4)$$

with the boundary condition $\alpha = 0$ at the wall. The correlation length scale is given by $L = C_L\, max\left(\frac{k^{3/2}}{\varepsilon}, C_\eta\left(\frac{\nu^3}{\varepsilon}\right)^{1/4}\right)$ with $C_L = 0.133$ and $C_\eta = 80$.

In Eq. (3), the ratio $k/R_i jn_in_j$ goes to infinity at the wall, which can lead to numerical instabilities in complex flows. Therefore, an alternative way of to writing $C'_{\varepsilon1}$ is used herein, introducing the non-equilibrium parameter $\frac{P}{\varepsilon}$,

$$C'_{\varepsilon1} = C_{\varepsilon1}\left[1+A_1^P\left(1-\alpha^3\right)\frac{P}{\varepsilon}\right], \quad (5)$$

with $A_1^P = 0.1$ and $C_L = 0.122$.

It is usual (see, for instance, Gunarjo, 2003; Kenjereš *et al.*, 2005) to use the same constant and time scale in the models for the terms P_ε and G_ε in Eq. 1, which leads to a model of the form $P_\varepsilon + G_\varepsilon = (P_k+G_k)/T$, as in Eq. 2. Since G_ε is due to buoyancy, while P_ε is a purely dynamic term, the variable coefficient $C'_{\varepsilon1}$, designed to reproduce the effect of the terms $P_{\varepsilon1}$, $P_{\varepsilon2}$ and $P_{\varepsilon3}$ is the near-wall region, should not be applied to G_ε, such that the model is recast as

$$P_\varepsilon + G_\varepsilon = C_{\varepsilon1}\left[1+A_1\left(1-\alpha^3\right)\frac{P}{\varepsilon}\right]\frac{P}{T}+C_{\varepsilon1}\frac{G}{T}. \quad (6)$$

Time scales

Moreover, the time scales for P_ε and G_ε can be considered the same only in case of a constant thermal-to-mechanical time-scale ratio, as is usually assumed far from the walls, but this simplification is not justified in general, in particular in near-wall regions.

For the dynamic production term P_ε, the choice of turnover time k/ε is standard, and, as suggested by Durbin (1991), this scale is bounded in the near-wall region by the Kolmogorov time scale as $T_d = max\left(\frac{k}{\varepsilon}, C_T\sqrt{\frac{\nu}{\varepsilon}}\right)$, with $C_T = 6$.

For buoyancy production, the thermal time scale $T_\theta = \overline{\theta'^2}/\varepsilon_\theta$ can be used instead of the dynamic time scale T_d.

Since the transport equation for ε_θ is not solved, the thermal time scale is obtained from

$$T_\theta = RT_d \ , \tag{7}$$

where R is the so-called thermal-to-mechanical time-scale ratio. The model for the production terms in the dissipation equation thus becomes

$$P_\varepsilon + G_\varepsilon = C_{\varepsilon 1}\left[1 + A_1^P\left(1-\alpha^3\right)\frac{P}{\varepsilon}\right]\frac{P}{T_d} + C_{\varepsilon 1}\frac{G}{RT_d}$$

For large turbulent Peclet numbers, which can be considered valid far from the wall, for fluids with not too small Prandtl numbers, assuming a constant thermal-to-mechanical time-scale ratio R is a usual practise Hanjalić (2002). For fluids with a Prandtl number close to unity, $R = 0.5$ is widely admitted. This R will be called R^h in the following (the superscript h denoting homogeneous or quasi-homogeneous).

However, this assumption fails in the near-wall region, where, in particular, R tends to the Prandtl number. In order to account for this limit, in the framework of the elliptic blending approach, R can be modelled as (Dehoux *et al.*, 2010, 2011)

$$R = (1-\alpha_\theta^3)Pr + R^h\alpha_\theta^3 \ . \tag{8}$$

This time scale ratio is denoted by $R(\alpha_\theta)$ in the remainder of the paper.

PRESENTATION OF THE COMPUTATIONS

EDF in-house open-source (http://www.code-saturne.org) CFD tool *Code_Saturne* is used for the present computations. *Code_Saturne* is an unstructured, collocated finite volume solver for cells of any shape. The Reynolds-averaged or filtered Navier-Stokes equations are solved for turbulent incompressible flows using a SIMPLEC algorithm for pressure-velocity coupling (for details, see Archambeau *et al.*, 2004). The EB-RSM, implemented as a near-wall extension of the SSG (Speziale *et al.*, 1991) model, is used for all the computations. As concerns Regarding the turbulent heat fluxes, the EB-AFM (Elliptic Blending-Algebraic Flux Model, already introduced in Lecocq *et al.*, 2008; Dehoux *et al.*, 2010, 2011) is used,

$$\overline{u_i'\theta'} = -C_\theta\frac{k}{\varepsilon}\left[\overline{u_i'u_j'}\frac{\partial\overline{\theta}}{\partial x_j} + \xi\overline{u_j'\theta'}\frac{\partial\overline{u_i}}{\partial x_j} + \eta\beta g_i\overline{\theta'^2} + \gamma\frac{\varepsilon}{k}\overline{u_j'\theta'}n_in_j\right] \ ,$$

with $C_\theta = \dfrac{0.68}{3\alpha_\theta^3 + (1-\alpha_\theta^3)C_\varepsilon}$, $\gamma = \left(1-\alpha_\theta^3\right)[1+C_\varepsilon]$, $C_\varepsilon = \dfrac{1}{2}\left(1+\dfrac{1}{\mathrm{Pr}}\right)$, $\xi = 1-0.55\alpha_\theta^3$ and $\eta = 1-0.55\alpha_\theta^3$ It is worth pointing out that, far from the wall, the model tends to the original AFM proposed by Hanjalić *et al.* (1996).

The equation for the temperature variance

$$\frac{\mathrm{D}\overline{\theta'^2}}{\mathrm{D}t} = \frac{\partial}{\partial x_k}\left[\left(\frac{\nu}{\mathrm{Pr}}\delta_{kl} + C_{\theta\theta}\,\rho\overline{u_k'u_l'}T\right)\frac{\partial\overline{\theta'^2}}{\partial x_l}\right] + P_\theta - \varepsilon_\theta \tag{9}$$

is solved, using

$$\varepsilon_\theta = \frac{\overline{\theta'^2}}{R(\alpha_\theta)}\frac{\varepsilon}{k} \ , \tag{10}$$

where the thermal-to-mechanical time-scale ratio $R(\alpha_\theta)$ is given by Eq. 8.

Table 1 gives an overview of the variants used to model the coefficients and the time scale entering the model for the dynamic and buoyancy production terms in the dissipation equation, under the general form

$$P_\varepsilon + G_\varepsilon = C_P P + C_G G \ . \tag{11}$$

Case 1 is the original formulation. In case 2, the ratio $\sqrt{k/R_{ij}n_in_j}$ is replaced by P/ε in $C_{\varepsilon 1}^{'}$, as explained above (see Eq. 5). In cases 3 to 6, the $C_{\varepsilon 1}$ coefficient is kept constant in the buoyancy production term (Eq. 6), and the modelling of the time scale is varied: for case 3, the standard dynamic time scale T_d is used; for cases 4 to 6 a thermal time scale T_θ is introduced, with different thermal-to-mechanical time-scale ratios. Note that the dynamic production term in case 5 is the same as in case 1, in order to test the validity of the time scale $R(\alpha_\theta)T_d$ with the original formulation of the dynamic production.

Table 1. The different constants and time scales used in the production term in ε equation ($P_\varepsilon = C_P P$, $G_\varepsilon = C_G G$, $\beta^k = A_1^k\left(1-\alpha^3\right)\sqrt{\frac{k}{R_{ij}n_in_j}}$, $\beta^P = A_1^P\left(1-\alpha^3\right)\frac{P}{\varepsilon}$)

	C_P	C_G
Case 1	$\frac{C_{\varepsilon 1}}{T_d}\left(1+\beta^k\right)$	$\frac{C_{\varepsilon 1}}{T_d}\left(1+\beta^k\right)$
Case 2	$\frac{C_{\varepsilon 1}}{T_d}\left(1+\beta^P\right)$	$\frac{C_{\varepsilon 1}}{T_d}\left(1+\beta^P\right)$
Case 3	$\frac{C_{\varepsilon 1}}{T_d}\left(1+\beta^P\right)$	$\frac{C_{\varepsilon 1}}{T_d}$
Case 4	$\frac{C_{\varepsilon 1}}{T_d}\left(1+\beta^P\right)$	$\frac{C_{\varepsilon 1}}{R^hT_d}$
Case 5	$\frac{C_{\varepsilon 1}}{T_d}\left(1+\beta^k\right)$	$\frac{C_{\varepsilon 1}}{R(\alpha_\theta)T_d}$
Case 6	$\frac{C_{\varepsilon 1}}{T_d}\left(1+\beta^P\right)$	$\frac{C_{\varepsilon 1}}{R(\alpha_\theta)T_d}$

RESULTS

Influence of the variable $C_{\varepsilon 1}$ coefficient

The comparison of case 2 and 3 with the baseline case (case 1) provides information about the influence of the variable coefficient in front of the production terms. The difference between case 1 and case 2 simply lies in the form of the

β function introduced to replicate the increase of production in the near-wall region due to $P_{\varepsilon 1}$, $P_{\varepsilon 2}$ and $P_{\varepsilon 3}$. In case 3, this function is simply set to zero, based on the remark that buoyancy production should not be directly affected by the increase of dynamic production. In Fig. 2, which shows the mean velocity in logarithmic scale, it can be seen that all these options lead to a strong over-estimation of the mean velocity, by more than 100%, similarly to was observed in the comparisons shown in Fig. 1, such that the incorrect introduction of a nonzero β function in the buoyancy term is not sufficient to explain the misprediction.

Fig. 3 gives the dissipation as a function of the distance to the wall in logarithmic scale. Although case 1 gives reasonable results for this variable, cases 2 and 3 show a completely unphysical dissipation level. Consequently, cases 2 and 3 show poor predictions of the other variables, since dissipation enters many terms of the model: for instance, dissipation and redistribution terms in the Reynolds stress equations involve ε, such that, as can be seen in Fig. 8, the shear stress is mispredicted in both the near-wall and central regions of the channel. The normal stresses are also affected by this over-estimation, which do not have a direct influence on the mean velocity, but on the time and length scales used in the transport equations for all the turbulent variables, via the kinetic energy (Fig. 7). The streamwise heat flux is also strongly over-estimated and the wall-normal heat flux is underestimated by a factor of 2 (Fig. 5), which is related to the underestimation of the mean temperature gradient at the wall (thus the Nusselt number).

It clearly appears from the comparison of case 1 and case 2 that the inclusion of the β term representing the role in the near-wall region of $P_{\varepsilon 1}$, $P_{\varepsilon 2}$ and $P_{\varepsilon 3}$ plays in the wrong direction, but the influence of the term is very limited and does not explain the wrong behaviour of the model. The use of the function β^k (case 1) leads to less wrong results, in particular concerning mean temperature (Fig. 4) and dissipation profiles (Fig. 3), but a large over-estimation of mean velocity (Fig. 2) and turbulent energy (Fig. 7) remains.

It will be seen in the following section that the poor behaviour of the models can be related to the use of the dynamic time scale in the buoyancy production term.

Influence of the time scale

The dynamic time scale, used in the buoyancy production G_ε for case 3, is replaced by a thermal time scale $T_\theta = \overline{\theta'^2}/\varepsilon_\theta$ for cases 4 and 6. Since the equation for ε_θ is not solved, the relation $T_\theta = RT_d$ is applied, where R is the thermal-to-mechanical time-scale ratio, such that the issue is now the modelling of R.

In case 4, R is simply considered a constant, with the value $R^h = 0.5$, widely accepted as the asymptotic limit in homogeneous situations, for fluids of Prandtl number close to unity, such that the modification is simply equivalent to an increase of the coefficient in front of the buoyancy production term. The effect on the predictions of the model is spectacular. In particular, the dissipation rate (Fig. 3) is drastically reduced compared to case 3. The mean velocity and temperature are clearly improved and all the second order moments have the correct order of magnitude. In particular, the prediction of the temperature variance (Fig. 6) is very satisfactory, but, has shown by the comparison with case 1, this quantity is not of fundamental importance for the global predictions of the model.

The comparison between case 6 and case 4 provides information about the importance of the reproduction of the increase (from 0.5 far from the wall to $Pr = 0.71$ at the wall) of the thermal-to-mechanical time-scale ratio in the near-wall region. In case 6, the ratio, denoted by $R(\alpha_\theta)$ is modelled by Eq. (8). Consistent with the previous observation about the role played by the value of the coefficient in front of the buoyancy production term, it is seen that the variation of R in the near-wall region has a significant impact on the predictions. Globally, the mean quantities are improved (mean velocity, Fig. 2, and mean temperature, Fig. 4), and consequently the quantities of engineering interest (friction coefficient and Nusselt number), although the turbulent energy, normal stresses and temperature variance are not improved everywhere (they are slightly improved in the near-wall region, but not far from the wall). It appears that a fine tuning of the coefficients used in case 6 could lead to a better reproduction of this flow, but such a calibration must be performed based on several flow configurations and is left to future work.

Finally, the comparison is made between cases 5 and 6 in order to check that, similar to the case of forced convection, the two formulations of the β function are exchangeable. It appears that the particular form of the function has an influence on the results, but, again, a fine tuning of the coefficients could make the predictions close to each other. Therefore, since the formulation β^P is numerically more robust, this version is recommended for future work.

CONCLUSION

Modelling the buoyancy production term in the turbulent dissipation equation was investigated for the natural convection regime. It was shown that introducing in the buoyancy production term the near-wall correction usually introduced for the dynamic production term is detrimental, consistent with the exact transport equation for the dissipation. Moreover, it has been shown that using the thermal time scale instead of the dynamic time scale yields a major improvement on the results for both first and second moments.

REFERENCES

Archambeau, F., Méchitoua, N. & Sakiz, M. 2004 Code Saturne: A finite volume code for the computation of turbulent incompressible flows - Industrial applications. *Int. J. on Finite Volume, Electronical edition: http://averoes.math.univ-paris13.fr/html* **ISSN 1634** (0655).

Dehoux, F., Benhamadouche, S. & Manceau, R. 2010 Modelling of the turbulent heat fluxes using elliptic blending. In *Proc. 8th ERCOFTAC Int. Symp. on Eng. Turb. Modelling and Measurements, Marseille, France*.

Dehoux, F., Lecocq, Y., Benhamadouche, S., Brizzi, L.-E. & Manceau, R. 2011 Algebraic modelling of the turbulent heat fluxes using the elliptic blending approach - application to forced and mixed convection regimes. *Flow Turbul. Combust.* Under revision.

Dol, H. S., Hanjalič, K. & Kenjereš, S. 1997 A comparative assessment in the second-moment differential and al-

gebraic models in turbulent natural convection. *Int. J. Heat Fluid Fl.* **18**, 4–14.

Durbin, P. A. 1991 Near-wall turbulence closure modeling without "damping functions". *Theor. Comput. Fluid Dyn.* **3**, 1–13.

Gunarjo, S. B. 2003 Contribution to advanced modelling of turbulent natural and mixed convection. PhD thesis, Technical University of Delft, The Netherlands.

Hanjalić, K. 2002 One-point closure models for buoyancy-driven turbulent flows. *Annu. Rev. Fluid Mech.* **34**, 321–347.

Hanjalić, K., Kenjereš, S. & Durst, F. 1996 Natural convection in partitioned two-dimensional enclosures at higher Rayleigh numbers. *Int. J. Heat Mass Tran.* **39** (7), 1407–1427.

Kasagi, N. & Nishimura, M. 1997 Direct numerical simulation of combined forced and natural turbulent convection in a vertical plane channel. *Int. J. Heat Fluid Fl.* **18** (1), 88–99.

Kenjereš, S., Gunarjo, S.B. & Hanjalić, K. 2005 Contribution to elliptic relaxation modelling of turbulent natural and mixed convection. *Int. J. Heat Fluid Fl.* **26** (4), 569–586.

Lecocq, Y., Manceau, R., Bournaud, S. & Brizzi, L.-E. 2008 Modelling of the turbulent heat fluxes in natural, forced and mixed convection regimes. In *Proc. 7th ERCOFTAC Int. Symp. on Eng. Turb. Modelling and Measurements, Limassol, Cyprus*.

Manceau, R. 2005 An improved version of the Elliptic Blending Model. Application to non-rotating and rotating channel flows. In *Proc. 4th Int. Symp. Turb. Shear Flow Phenomena, Williamsburg, VA, USA*.

Manceau, R. & Hanjalić, K. 2002 Elliptic blending model: A new near-wall Reynolds-stress turbulence closure. *Phys. Fluids* **14** (2), 744–754.

Shin, J. K., An, J. S., Choi, Y. D., Kim, Y. C. & Kim, M. S. 2008 Elliptic relaxation second moment closure for the turbulent heat fluxes. *J. Turbul.* **9** (3), 1–29.

Speziale, C. G., Sarkar, S. & Gatski, T. B. 1991 Modeling the pressure-strain correlation of turbulence: an invariant dynamical system approach. *J. Fluid Mech.* **227**, 245–272.

Thielen, L., Hanjalić, K., Jonker, H. & Manceau, R. 2005 Predictions of flow and heat transfer in multiple impinging jets with an elliptic-blending second-moment closure. *Int. J. Heat Mass Tran.* **48** (8), 1583–1598.

Versteegh, T. A. M. & Nieuwstadt, F. T. M. 1999 A direct numerical simulation of natural convection between two infinite vertical differentially heated walls scaling laws and

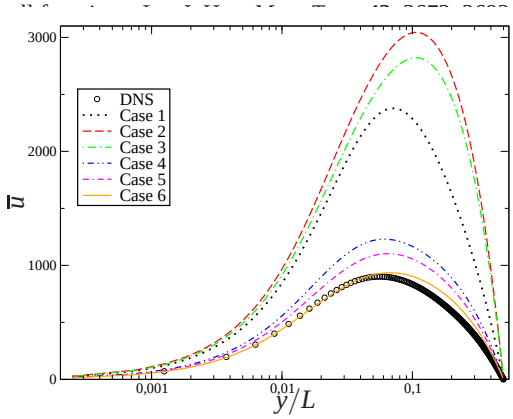

Figure 2. Mean velocity

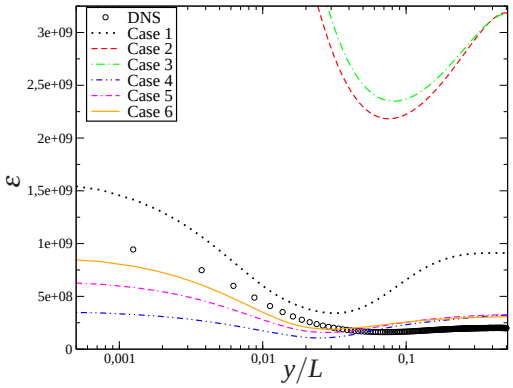

Figure 3. Dissipation rate

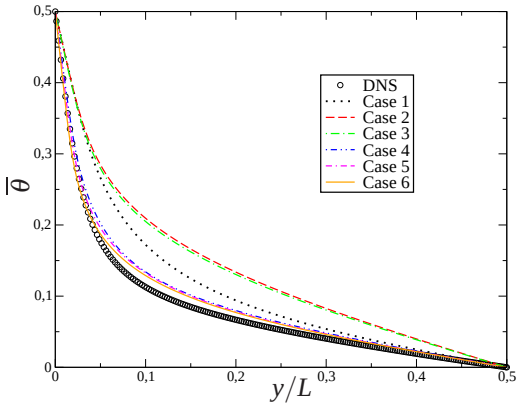

Figure 4. Mean temperature

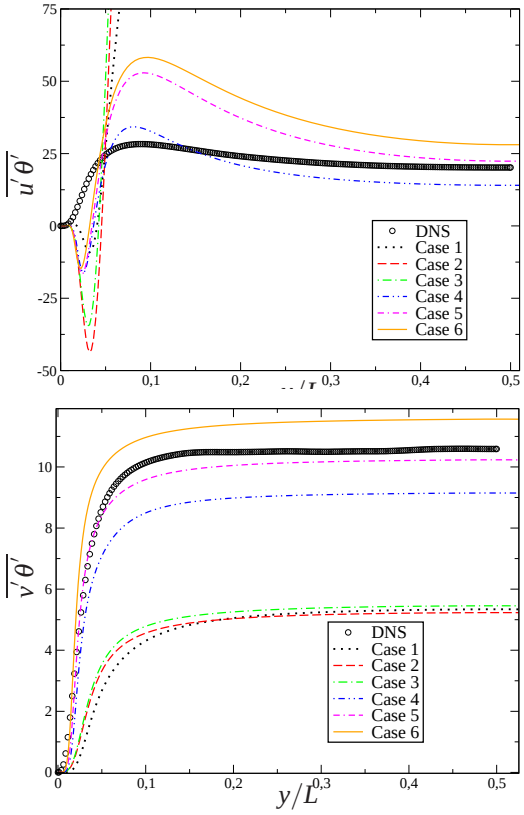

Figure 5. Turbulent heat fluxes

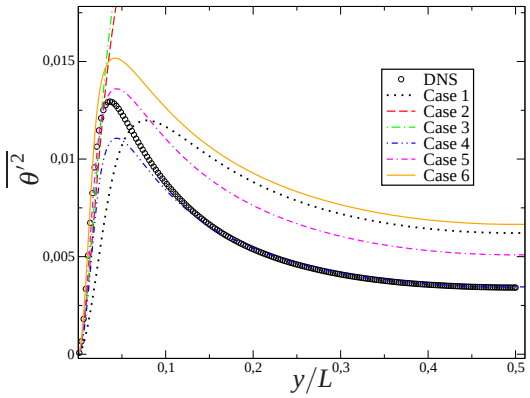

Figure 6. Temperature variance

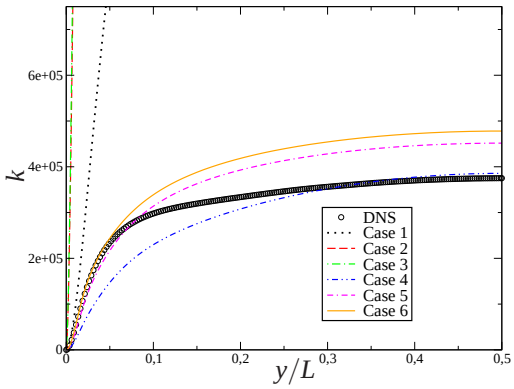

Figure 7. Turbulent kinetic energy

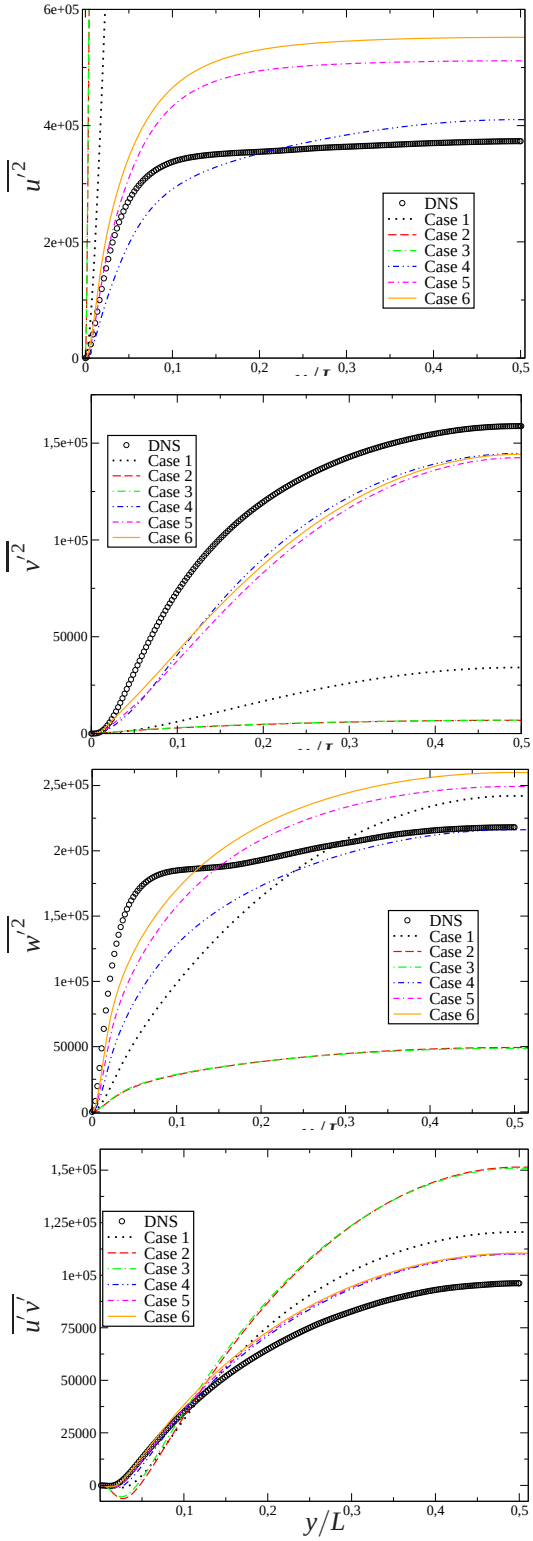

Figure 8. Reynolds stresses